Research Article | Vol. 27, No. 13 | 24 Jun 2019 | OPTICS EXPRESS 17426
Optics EXPRESS

Compressed sensing of twisted photons

FRÉDÉRIC BOUCHARD,[1] DOMINIK KOUTNÝ,[2] FELIX HUFNAGEL,[1] ZDENĚK HRADIL,[2] JAROSLAV ŘEHÁČEK,[2] YONG-SIAH TEO,[3] DAEKUN AHN,[3] HYUNSEOK JEONG,[3] LUIS L. SÁNCHEZ-SOTO,[4,5,*] GERD LEUCHS,[1,5] AND EBRAHIM KARIMI[1,5]

[1]*Department of Physics, University of Ottawa, 25 Templeton Street, Ottawa, Ontario, K1N 6N5, Canada*
[2]*Department of Optics, Palacký University, 17. listopadu 12, 771 46 Olomouc, Czech Republic*
[3]*Department of Physics and Astronomy, Seoul National University, 08826 Seoul, South Korea*
[4]*Departamento de Óptica, Facultad de Física, Universidad Complutense, 28040 Madrid, Spain*
[5]*Max-Planck-Institut für die Physik des Lichts, Staudtstraße 2, 91058 Erlangen, Germany*
[*]*lsanchez@fis.ucm.es*

Abstract: The ability to completely characterize the state of a system is an essential element for the emerging quantum technologies. Here, we present a compressed-sensing-inspired method to ascertain any rank-deficient qudit state, which we experimentally encode in photonic orbital angular momentum. We efficiently reconstruct these qudit states from a few scans with an intensified CCD camera. Since it only requires a small number of intensity measurements, our technique provides an easy and accurate way to identify quantum sources, channels, and systems.

1. Introduction

The orbital angular momentum (OAM) of single photons, which provides an unbounded vector space, has been recognized as a preeminent platform for encoding both quantum [1–3] and classical [4, 5] information. Although the generation of photons with OAM is relatively simple, the full characterization of a state in the OAM Hilbert space stands as a challenging task. Several methods have demonstrated accurate projective measurements to determine OAM states [6–11]. However, these projective measurements work adequately only for pure states. The case of mixed states requires full state tomography, and this involves projective measurements on arbitrary superpositions of two or more OAM eigenstates [12], a task which remains challenging.

To circumvent these problems, we propose and experimentally demonstrate a method inspired by compressed sensing. Originating from the context of classical signal processing [13, 14], this technique harnesses prior assumptions about the state to reconstruct it from an undersampled set of measurements. It is routinely used to estimate vectors or matrices from incomplete information, with applications in many diverse fields of research [15, 16]. Compressed sensing has also been adapted as a tool for state tomography of discrete systems in quantum theory [17–24].

The primary goal of our scheme for reconstructing OAM states is to significantly reduce the number of z-axis scans (Z) given an *a priori* value of the mode rank s. We shall demonstrate that intensity measurement with only a small Z (thus giving n_Z number of linearly independent detection outcomes) is sufficient to unambiguously reconstruct OAM states of low rank s, which constitutes our main result. Actually, the compressed sensing algorithms, supplemented with the positivity constraint [25], which operates as a kind of regularization, enables us to construct informationally complete measurements that are robust to noise and modeling errors. In other words, one can use a very simple setup for the characterization of a state with *a priori* information about its nature.

#352203 https://doi.org/10.1364/OE.27.017426
Journal © 2019 Received 19 Nov 2018; revised 21 May 2019; accepted 22 May 2019; published 10 Jun 2019

Optics EXPRESS

2. Setting the scenario

We begin our analysis by recalling a few basic concepts that we will need to understand the technique. We are dealing with single photons carrying OAM, which has made this degree of freedom an ideal candidate for the investigation of complex quantum phenomena and their applications. For this reason, we describe the OAM modes in a quantum parlance, although everything can be immediately translated into a classical framework.

In any tomographic protocol, one infers the state, represented by the density matrix ϱ, from the distinct outcomes of a collection of measurements performed on identical copies of the system. The outcomes of these measurements are given by the Born rule $p_\alpha = \mathrm{Tr}(\varrho\,\Pi_\alpha)$, where $\{\Pi_\alpha\}$ is the positive operator-valued measure (POVM) describing the setup [26]. We denote the action of the POVM by $\mathcal{A} : \varrho \mapsto \mathbf{p}$, that maps ϱ onto the vector containing all the probabilities $\{p_\alpha\}$.

A POVM is informationally complete (IC) when the corresponding outcome probabilities are sufficient to determine an arbitrary state [27, 28]. Obviously, the number of outcomes of any IC measurement is at least d^2, where d is the dimension of the system, which makes traditional methods infeasible as d increases. However, if we know *a priori* that the rank of the system fulfills $\mathrm{rank}(\varrho) \leq s$, with $s \ll d$, then we can substantially reduce the number of measurement samples required to uniquely reconstruct the unknown signal matrix. It has been shown that for any map $\mathcal{A}$, the so-called restricted isometry property [29] (which characterizes matrices that are nearly orthonormal, at least when operating on sparse vectors is sufficient to yield a unique rank-s reconstruction: the true state ϱ_0 is then the only density matrix within the set of positive Hermitian matrices of any rank that yields the measurement probabilities $\mathbf{p}$ [25]. The corresponding estimator $\widehat{\varrho}$ for ϱ_0, based on collected statistical data, is given by

$$\widehat{\varrho} = \min_{\varrho} \|\mathcal{A}[\varrho] - \mathbf{p}\| \quad \text{subject to} \quad \varrho \geq 0\,, \tag{1}$$

whose solution can be efficiently found by convex programming [30].

The insights into the regularizing effect of the positivity constraint permit us to tackle reconstructing OAM quantum states. To represent the structure of the transverse field we will be using the well-known Laguerre-Gauss (LG) modes that can be written as [31],

$$\begin{aligned}\mathrm{LG}_{p\ell}(r,\phi,z) = \langle r,\phi,z|\,\ell,p\rangle = \sqrt{\frac{2p!}{\pi(p+|\ell|)!}}\,\frac{1}{w(z)}\left(\frac{\sqrt{2}r}{w(z)}\right)^{|\ell|}\\ \times L_p^{|\ell|}\left(\frac{2r^2}{w(z)^2}\right)\exp\left(-r^2\left[\frac{1}{w(z)^2} - i\frac{k}{2R(z)}\right] - i\ell\phi - i\psi_{p\ell}(z)\right),\end{aligned} \tag{2}$$

where (r,ϕ,z) denote cylindrical coordinates, k is the wave number, $L_p^{|\ell|}(.)$ is the generalized Laguerre polynomial, $\ell \in \{0, \pm1, \pm2, \ldots\}$ is the azimuthal mode index, and $p \in \{0, 1, 2, \ldots\}$ is the radial mode index, which is related to the number of radial nodes. The parameters $R(z)$, $w(z)$, and $\psi_{p\ell}(z)$ denote the radius curvature of the wave fronts, the beam radius, and the Gouy phase at the propagation distance z, respectively:

$$\begin{aligned} w^2(z) &= w_0^2\left[1 + (z/z_\mathrm{R})^2\right],\\ R(z) &= z\left[1 + (z_\mathrm{R}/z)^2\right],\\ \psi_{p\ell}(z) &= (2p + |\ell| + 1)\arctan(z/z_R),\end{aligned} \tag{3}$$

with the Rayleigh range $z_\mathrm{R} = kw_0^2/2$ and w_0 the beam waist, which we assume located at $z = 0$. In what follows, we will set $p = 0$ and denote $\psi_\ell(z) = \psi_{p=0\,\ell}(z)$.

We propose to reconstruct the signal in the LG basis from Z intensity scans registered by a CCD camera positioned at distances $z_1, z_2, \ldots$, with respect to the beam waist, which is in the

Optics EXPRESS

spirit of the Gerchberg-Saxton algorithm [32]. This amounts to projecting the density matrix on free-space position eigenstates; viz,

$$p(r,\phi,z) = \langle r,\phi,z|\varrho|r,\phi,z\rangle = \sum_{\ell,\ell'} \mathrm{LG}_{\ell,0}(r,\phi,z)\,\varrho_{\ell\ell'}\,\mathrm{LG}^{*}_{\ell',0}(r,\phi,z) \propto e^{-2\mathfrak{r}^2} \sum_{\ell\ell'} \varrho_{\ell\ell'}\,C_{\ell\ell'}, \quad (4)$$

where

$$C_{\ell\ell'} = \mathfrak{r}^{|\ell|+|\ell'|} \exp[i(\ell-\ell')\phi] \exp\{i[\psi_\ell(z) - \psi_{\ell'}(z)]\}, \qquad \mathfrak{r}(z) = r/w(z). \quad (5)$$

Each combination of r, ϕ, and z coordinates, which corresponds to the associated pixel readings, gives us one particular linear combination of density matrix elements. Evidently by varying r, ϕ, and z, the more linearly independent these generated combinations are, the more IC the POVM is.

3. Informational completeness of intensity scans

The aim of compressed sensing is to perform a set of IC POVM measurement outcomes to uniquely reconstruct the unknown state ϱ. In our context of twisted-photon state reconstruction, the POVM refers to the set of CCD intensity scans along the propagation axis. In this section, we shall analytically demonstrate that a few CCD scans shall be needed to unambiguously, and thus compressively, reconstruct an arbitrary d-dimensional state under various conditions on the angular momentum quantum number ℓ. To simplify the details as much as possible, we will ignore statistical noise and take $p(r,\phi,z)$ to represent the raw data. We also assume there are no limits on sampling in r and ϕ coordinates.

First, we consider d-dimensional signals represented by LG beams with nonnegative azimuthal indexes only $\ell \in \{0,1,\cdots,d-1\}$. We will show that a single CCD scan provides complete information about the signal. In this case (for a fixed z) one can ignore the Gouy's phase. Obviously, incompleteness arises whenever two different pairs (ℓ',ℓ'') generate the same $C_{\ell'\ell''}$ for all r and ϕ. Since for $\ell',\ell'' \geq 0$, we have $|\ell'| - |\ell''| = \ell' - \ell''$, there just cannot be two such pairs both satisfying $\ell' - \ell'' = N$ and $\ell' - \ell'' = M$ with the same N and M and incompleteness does not arise. Hence, all density matrix elements can be uniquely determined from a single CCD scan for any dimension d of our system.

When the sign of the topological charge is not constrained, the space dimension is $d = 2\ell_{\max}+1$, so that $\ell \in \{-\ell_{\max},\cdots,0,\cdots,\ell_{\max}\}$. Now, the CCD scans are no longer IC no matter how many planes Z are sampled. Indeed, incompleteness arises when two or more elements $C_{\ell'\ell''}$ coincide for all r, ϕ and z. This requires

$$|\ell'| - |\ell''| = N, \qquad \ell' - \ell'' = M, \qquad |\ell'| - |\ell''| = S, \quad (6)$$

to hold for two or more distinct pairs (ℓ',ℓ''). For every $0 < n \leq \ell_{\max}$ one finds two such realizations: $\ell',\ell'' = n$ and $\ell',\ \ell'' = -n$ and as a result states $|\ell\rangle$ and $|-\ell\rangle$ cannot be discriminated by intensity measurements alone. As there are $\ell_{\max}$ such cases, the maximum number of linearly independent measurements generated by CCD scans in dimension d is

$$n_{Z\to\infty} = 4{\ell_{\max}}^2 + 4\ell_{\max} + 1 = d^2 - \tfrac{1}{2}(d-1)\,. \quad (7)$$

For large dimensions $d^2 \gg d$ and the measurement setup becomes nearly complete.

Let us explore how the set of independent detections builds up. For a single plane, the Gouy's phase and hence relation (6) are of no consequence. The number of independent detections equals the number of distinct couples (N,M) that can be generated by $-\ell_{\max} \leq \ell',\ \ell'' \leq \ell_{\max}$. It can be checked that for a given N, each pair of nonnegative indexes $\ell',\ell'' \geq 0$, $|\ell'| + |\ell''| = N$ generates a unique (N,M). Negative $\ell',\ell'' < 0$ do not add new entries to this set. Finally, there are only two possible Ms for all pairs with opposite signs $M = \ell' - \ell'' = \ell' + (-\ell'') = \pm N$. When $N \leq \ell_{\max}$ these are already accounted for by $\ell' = 0$, $\ell'' = N$ and $\ell' = N$, $\ell'' = 0$ appearing

Optics EXPRESS

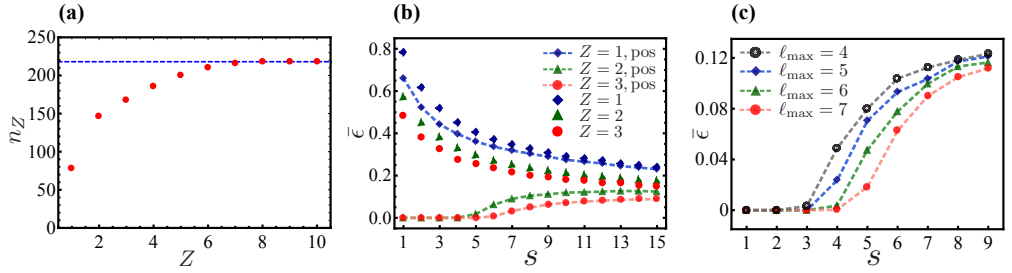

Fig. 1. Simulation of our compressed sensing protocol with twisted photons. (a) Number of independent detections n_Z generated by Z intensity scans along the propagation axis performed on a signal with $\ell_{\max} = 7$ ($d = 15$). The maximum of $n_Z = 218$ detections is obtained for $Z \geq 8$ scans. (b) Reconstructions errors, $\bar{\varepsilon}$, from the compressed sensing protocol of the twisted photons as a function of the rank of the state for a fixed dimension ($\ell_{\max} = 7$) and for $Z = 1, 2$, and 3 CCD scans, with and without positivity constraint. (c) The reconstructions errors for two CCD scans and different dimensions. In all the cases, we take a 19×19 pixels screen.

in the set of nonnegative pairs. When $N > \ell_{\max}$, the values $M = \pm N$ make new entries. This gives $\sum_{\ell'=0}^{N} \sum_{\ell''=0}^{\ell_{\max}} \delta_{\ell'',N-\ell'} = N + 1$ entries for $N \leq \ell_{\max}$ and $2 + \sum_{\ell'=N-\ell_{\max}}^{\ell_{\max}} \sum_{\ell''=0}^{\ell_{\max}} \delta_{\ell'',N-\ell'} = 2\ell_{\max} - N + 3$ entries for $N > \ell_{\max}$. Taking sum over $N = 0 \ldots 2\ell_{\max}$ this makes a total of

$$n_{Z=1} = {\ell_{\max}}^2 + 4\ell_{\max} + 1 = \tfrac{1}{4}(d^2 + 6d - 3) \tag{8}$$

independent detections generated by a single intensity scan—about a quarter of the maximum number of independent detections (7).

Going further, we realize that each couple (N, M) is degenerate; i.e., can be generated by at least two distinct pairs (ℓ', ℓ''), except for $(N = 0, M = 0)$, and $(N = \ell_{\max}, M = \pm\ell_{\max})$. In addition, degenerate $(N > 0, M = 0)$ cannot be resolved by additional scans, as we have already discussed. Hence, the second scan adds $\Delta n_{Z=2} = {\ell_{\max}}^2 + 4\ell_{\max} + 1 - (3 + \ell_{\max}) = {\ell_{\max}}^2 + 3\ell_{\max} - 2$ additional independent detections, bringing the total for two scans to

$$n_{Z=2} = 2{\ell_{\max}}^2 + 7\ell_{\max} - 1 = \tfrac{1}{2}(d^2 + 5d - 8)\,. \tag{9}$$

For higher Z, the new independent detections grow linearly with $\ell_{\max}$. A typical behaviour is shown in Fig. 1(a) for $\ell_{\max} = 7$: the maximum $n_{Z\to\infty}$ is approximately attained with 8 scans. Actually, the minimum scans required to approximately attain the maximum number of independent detections in the signal space is $Z_{\min} = \ell_{\max} + 1$.

The compressive tomography is done by solving (1), where now $\alpha = \{r, \phi, z\}$, and Π_α is defined by $\mathrm{Tr}(\varrho\,\Pi_\alpha) = p(r, \phi, z)$. We first perform numerical simulations to explore the method. A set of random states of a given rank in the $\ell_{\max} = 7$ space is chosen and scanning measurements are simulated for $Z = 1$, 2, and 3 CCD planes with a 19×19 pixel geometry.

The data is subject to state reconstruction with and without the positivity constraints, where the latter is implemented with the help of the Moore-Penrose pseudoinverse [33]. Finally, for each true state, the corresponding Hilbert-Schmidt distances between the true and reconstructed states are calculated and the mean is taken over the set of true states of the same rank [34]. We take this as the error $\bar{\varepsilon} = \mathbb{E}[\mathrm{Tr}(\varrho_{\mathrm{true}} - \widehat{\varrho})^2]$.

In Fig. 1(b), we have plotted the errors $\bar{\varepsilon}$ as a function of the rank of the state, for $\ell_{\max} = 7$. We observe a strong regularizing effect of the positivity constraint, especially on low-rank signals. First, positivity always makes the reconstruction errors smaller. Second, it cures the informational incompleteness of the tomography, provided the complexity of the measured signal stays below a

Optics EXPRESS

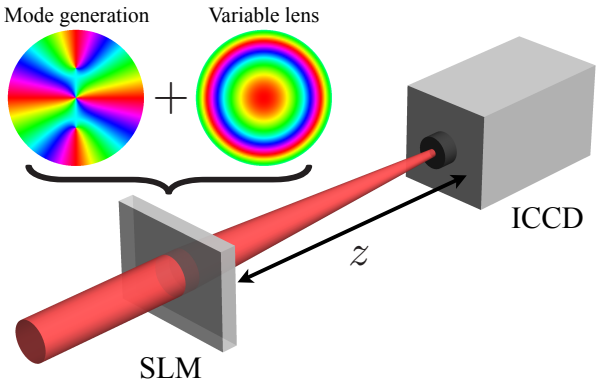

Fig. 2. Sketch of the experimental setup. A photonic state is generated by manipulating the phase and intensity of an incoming beam via the spatial light modulator (SLM). The beam is then focused using a variable holographic lens imprinted on the SLM together with the state generation hologram. The ICCD camera has a fixed position and records intensity scans. Inset shows the state and lens phase patterns, $[0, 2\pi)$, in a hue color.

certain threshold. Last, this threshold gets increased as we collect more scans. Notice though that protocols with positivity perform worse on more complex signals because the regularizing effect of positivity weakens. Loosely speaking, in comparing neighbourhoods of low- and high-rank states, one finds more nonphysical matrices in the former. Those objects get filtered by the positivity constraints leading to improved performance. The opposite is true of the protocols without positivity. Here, the more mixed states are less biased in the space of density matrices, so their average distance to the reconstructed matrix is smaller. Notice that this discussion does not apply to mutually compatible observations, for which positivity constraints are of no consequence. This can be observed in Fig. 1(c) for a single scan, where the regularizing effect of positivity disappears. Stronger incompatibilities introduced by detections from different planes $[\Pi_\alpha, \Pi_{\alpha'}] \neq 0$ are required to promote signal sparsity. The influence of the signal dimension with a fixed measurement is also illustrated in Fig. 1(c), for the particular case of two scans. The quality of the compressive OAM tomography improves with the signal dimension. At first glance, this might seem counterintuitive; however, note that the sparsity of a signal of a given rank grows with dimension and so do the regularizing effects of positivity constraints.

4. Experiment

To verify our scheme, we construct an experimental setup that allows us to generate and detect vortex beams at the single photon level using a spatial light modulator (SLM) and an intensified CCD (ICCD camera, respectively. A simplified sketch is shown in Fig. 2. A quasi-continuous UV laser, at a wavelength of 355 nm, is used to pump a type-I β-barium borate (BBO) crystal in order to generate single photons via spontaneous parametric downconversion. The spatial modes of the generated photons are filtered to the fundamental Gaussian mode by coupling them to a single mode fibre (SMF). A coincidence rate of 30 kHz and singles rate of 200 kHz is measured after the SMF. The photons are then coupled out of the SMF and are made incident on an SLM, (X10468-07, Hamamatsu) consisting of an electronically controlled nematic liquid crystal device with 792×600 pixels. The phase and the intensity of the generated photons are controlled via a holographic intensity masking technique [35], with a diffraction efficiency greater than 70 %. To achieve a higher mode quality, a $10\times$ microscope objective with a numerical aperture of 0.25 is employed to obtain a relatively large collimated beam at the SLM. The mode waist of the amplitude-modulated hologram at the SLM is determined to have an effectively flat phase and

Optics EXPRESS

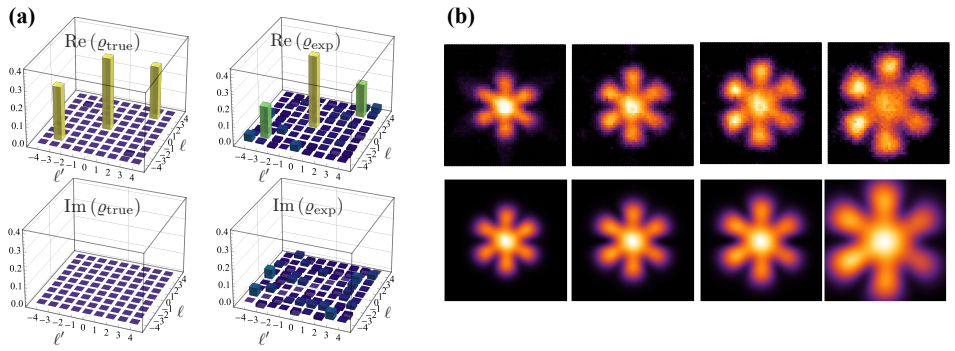

Fig. 3. Experimental reconstruction from compressed sensing. (a) Density matrix of the true state and (b) Reconstructed density matrix after two intensity scans with a signal space spanned by $\ell \in \{-4, \ldots, 4\}$. The upper row shows four experimental ICCD scans at the planes z/z_R =0, 1/3, 1/2, and 1, respectively. The lower row shows the predictions from the reconstructed state of the same ICCD scans.

intensity for the incoming beam over the region of interest of the hologram. By doing so, we may generate any arbitrary spatial mode with a high-level of accuracy. In the case of pure states, a single hologram is used for shaping the transverse modes of all photons in the ensemble. For mixed states, the appropriate holograms are randomly varied to generate incoherent statistical mixtures of the desired modes. A single intensity scan is then recorded over the whole ensemble of generated photons.

To observe the intensity variation of LG modes upon propagation, due to the differences in Gouy phases, the beam must propagate for distances that are on the order of the Rayleigh range z_R. This is achieved by simply focusing the beam. In the scheme described above, the ICCD camera is moved along the path of the beam in the z-direction. However, this is equivalent to varying the focal length of the lens and considering a fixed position of the ICCD camera. This is accomplished by imprinting a phase profile of the form $\exp\left(-i\,k\,r^2/2f\right)$, where f is the focal length of the flat lens. By doing so, our experimental reconstruction does not require any mechanical displacement of the components in the setup. Intensity scans are recorded for different focal lengths corresponding to positions of z/z_R = 0, 1/3, 1/2 and 1. Finally, both coincidence

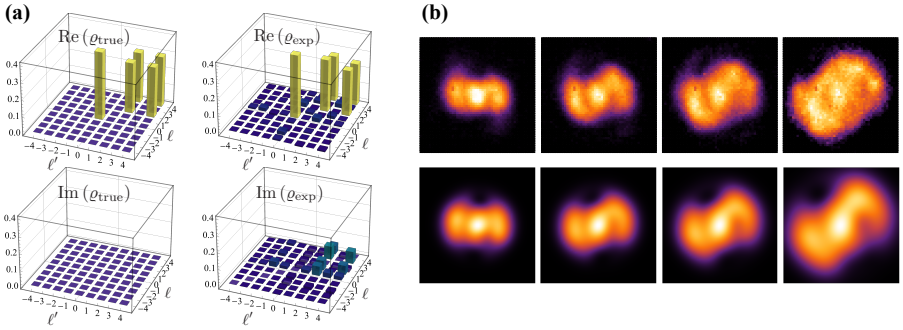

Fig. 4. Experimental reconstruction from compressed sensing. (a) Density matrix of the true state and (b) Reconstructed density matrix after one intensity scan. The upper row shows four experimental ICCD scans at the planes z/z_R =0, 1/3, 1/2, and 1, respectively. The lower row shows the predictions from the reconstructed state of the same ICCD scans.

Optics EXPRESS

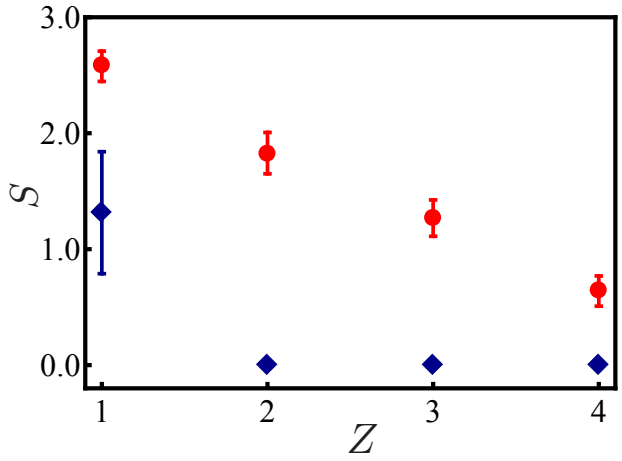

Fig. 5. Entropy S as a function of the number of intensity scans Z, for a signal space spanned by $\ell \in \{-4, \ldots, 4\}$ and for true states of the form in (10). The circles are obtained by averaging over 20 random states and the error bars indicate the corresponding variance. Blue refers to protocol with positivity, while red is without positivity.

and singles counts measurements can be recorded with the ICCD camera. However, since we do not make use of the spatial correlation resulting from spontaneous parametric downconversion, the ICCD camera is used without triggering, where shorter integration time may be considered.

The true states are chosen to be following rank–2 states,

$$\varrho = p\,|0\rangle\langle 0| + (1-p)\,|\Psi\rangle\langle\Psi|, \tag{10}$$

with $|\Psi\rangle = \cos\theta\ |-3\rangle + \sin\theta\ |3\rangle$. In the experiment, we randomly generate 20 states for values of p and θ chosen. The OAM mixed states are generated by randomly varying the holograms displayed on the SLM. The holograms corresponding to the states $|0\rangle$ and $|\Psi\rangle$ are displayed for a fraction of the total integration time corresponding to p and $(1-p)$, respectively. In Fig. 3, we present the results for a typical state ϱ with two ICCD scans. The corresponding reconstructed density matrix is plotted in the left column. Even though we are dealing with informationally incomplete measurements, the protocol with positivity using two intensity scans fits the theoretical data quite well. Without the positivity constraint, the reconstructed states are very different from the true ones. We have also experimentally checked that when the signal space is constrained to only positive topological charges ℓ, one intensity scan is enough to accurately predict the intensity scans in other planes, as anticipated by our theory.

We have also considered another set of rank–2 states, similar to Eq. (10), but now with $|\Psi\rangle = \cos\theta\,|2\rangle + \sin\theta\,|4\rangle$. The results are presented in Fig. 4. The reconstructed density matrix is plotted in the left column. We have also experimentally checked that when the signal space is constrained to only positive topological charges ℓ, one intensity scan is enough to accurately predict the intensity scans in other planes, as anticipated by our theory.

To assess the degree of IC for the intensity scans, we first consider a matrix of reconstructed states $\{\widehat{\varrho}_j\}$ with its jth column defined as a flattened ϱ_j. A unique solution for the extremal problem Eq.(1) then implies that the entropy of normalized singular values for this matrix is zero. To compute the entropy, we reconstructed 20 true states for every ICCD scan, and average over all of them. As can be seen in Fig. 5, the protocol with positivity constraints is enough to characterize the input state with solely two scans. We corroborate once again that if we restrict our space to be spanned only with nonnegative azimuthal indices, the measurement is IC for both strategies (with and without positivity) with only one intensity scan.

Optics EXPRESS

5. Concluding remarks

In summary, we have developed a compressed sensing scheme able to uniquely reconstruct any rank-deficient qudit state encoded in the OAM degree of freedom. The positivity constraint has played a substantial role as a powerful regularization to perform a tomographic reconstruction in the regime of informationally incomplete data for intermediately sized quantum systems. This establishes a novel and efficient tomographic paradigm for OAM systems that could trigger interesting experimental research on complex quantum states, which otherwise might have been infeasible with currently known detection schemes in such experiments.

Funding

European Union's Horizon 2020 Research and Innovation Programme (766970); Canada Research Chairs; Ontario's Early Researcher Award; BK21 Plus Program (21A20131111123); National Research Foundation of Korea (2010-0018295); Korea Institute of Science and Technology Institutional Program (2E27800-18-P043); Ministerio de Economía y Competitividad (FIS2015-67963-P); Grant Agency of the Czech Republic (18-04291S); Internal Grant Agency of the Faculty of Sciences of Palacký University (PrF 2018-003)

References

1. G. Vallone, V. D'Ambrosio, A. Sponselli, S. Slussarenko, L. Marrucci, F. Sciarrino, and P. Villoresi, "Free-space quantum key distribution by rotation-invariant twisted photons," Phys. Rev. Lett. **113**, 060503 (2014).
2. M. Mirhosseini, O. S. Magaña-Loaiza, M. N. O'Sullivan, B. Rodenburg, M. Malik, M. P. J. Lavery, M. J. Padgett, D. J. Gauthier, and R. W. Boyd, "High-dimensional quantum cryptography with twisted light," New J. Phys. **17**, 033033 (2015).
3. A. Sit, F. Bouchard, R. Fickler, J. Gagnon-Bischoff, H. Larocque, K. Heshami, D. Elser, C. Peuntinger, K. Günthner, B. Heim, C. Marquardt, G. Leuchs, R. W. Boyd, and E. Karimi, "High-dimensional intracity quantum cryptography with structured photons," Optica **4**, 1006–1010 (2017).
4. G. Gibson, J. Courtial, M. J. Padgett, M. Vasnetsov, V. Pas'ko, S. M. Barnett, and S. Franke-Arnold, "Free-space information transfer using light beams carrying orbital angular momentum," Opt. Express **12**, 5448–5456 (2004).
5. J. Wang, J.-Y. Yang, I. M. Fazal, N. Ahmed, Y. Yan, H. Huang, Y. Ren, Y. Yue, S. Dolinar, M. Tur, and A. E. Willner, "Terabit free-space data transmission employing orbital angular momentum multiplexing," Nat. Photonics **6**, 488 (2012).
6. A. Mair, A. Vaziri, G. Weihs, and A. Zeilinger, "Entanglement of the orbital angular momentum states of photons," Nature **412**, 313 (2001).
7. J. Leach, M. J. Padgett, S. M. Barnett, S. Franke-Arnold, and J. Courtial, "Measuring the orbital angular momentum of a single photon," Phys. Rev. Lett. **88**, 257901 (2002).
8. J. Leach, J. Courtial, K. Skeldon, S. M. Barnett, S. Franke-Arnold, and M. J. Padgett, "Interferometric methods to measure orbital and spin, or the total angular momentum of a single photon," Phys. Rev. Lett. **92**, 013601 (2004).
9. E. Karimi, B. Piccirillo, E. Nagali, L. Marrucci, and E. Santamato, "Efficient generation and sorting of orbital angular momentum eigenmodes of light by thermally tuned q-plates," Appl. Phys. Lett. **94**, 231124 (2009).
10. G. C. G. Berkhout, M. P. J. Lavery, J. Courtial, M. Beijersbergen, and M. J. Padgett, "Efficient sorting of orbital angular momentum states of light," Phys. Rev. Lett. **105**, 153601 (2010).
11. M. Mirhosseini, M. Malik, Z. Shi, and R. W. Boyd, "Efficient separation of the orbital angular momentum eigenstates of light," Nat. Commun. **4**, 2781 (2013).
12. N. Bent, H. Qassim, A. A. Tahir, D. Sych, G. Leuchs, L. L. Sánchez-Soto, E. Karimi, and R. W. Boyd, "Experimental realization of quantum tomography of photonic qudits via symmetric informationally complete positive operator-valued measures," Phys. Rev. X **5**, 041006 (2015).
13. E. J. Candes, J. Romberg, and T. Tao, "Robust uncertainty principles: exact signal reconstruction from highly incomplete frequency information," IEEE Trans. Inform. Theory **52**, 489–509 (2006).
14. E. J. Candes and T. Tao, "The power of convex relaxation: Near-optimal matrix completion," IEEE Trans. Inf. Theory **56**, 2053–2080 (2010).
15. Y. C. Eldar and G. Kutyniok, *Compressed Sensing: Theory and Applications* (Cambridge University, 2012).
16. A. Stern, *Optical Compressive Imaging* (CRC, 2016).
17. D. Gross, Y.-K. Liu, S. T. Flammia, S. Becker, and J. Eisert, "Quantum state tomography via compressed sensing," Phys. Rev. Lett. **105**, 150401 (2010).
18. A. Shabani, R. L. Kosut, M. Mohseni, H. Rabitz, M. A. Broome, M. P. Almeida, A. Fedrizzi, and A. G. White, "Efficient measurement of quantum dynamics via compressive sensing," Phys. Rev. Lett. **106**, 100401 (2011).
19. W.-T. Liu, T. Zhang, J.-Y. Liu, P.-X. Chen, and J.-M. Yuan, "Experimental quantum state tomography via compressed sampling," Phys. Rev. Lett. **108**, 170403 (2012).

Optics EXPRESS

20. C. Schwemmer, G. Tóth, A. Niggebaum, T. Moroder, D. Gross, O. Gühne, and H. Weinfurter, "Experimental comparison of efficient tomography schemes for a six-qubit state," Phys. Rev. Lett. **113**, 040503 (2014).
21. A. V. Rodionov, A. Veitia, R. Barends, J. Kelly, D. Sank, J. Wenner, J. M. Martinis, R. L. Kosut, and A. N. Korotkov, "Compressed sensing quantum process tomography for superconducting quantum gates," Phys. Rev. B **90**, 144504 (2014).
22. F. Tonolini, S. Chan, M. Agnew, A. Lindsay, and J. Leach, "Reconstructing high-dimensional two-photon entangled states via compressive sensing," Sci. Rep. **4**, 6542 (2014).
23. A. Steffens, C. A. Riofrío, W. McCutcheon, I. Roth, B. A. Bell, A. McMillan, M. S. Tame, J. G. Rarity, and J. Eisert, "Experimentally exploring compressed sensing quantum tomography," Quantum Sci. Technol. **2**, 025005 (2017).
24. C. A. Riofrío, D. Gross, S. T. Flammia, T. Monz, D. Nigg, R. Blatt, and J. Eisert, "Experimental quantum compressed sensing for a seven-qubit system," Nat. Commun. **8**, 15305 (2017).
25. A. Kalev, R. L. Kosut, and I. H. Deutsch, "Quantum tomography protocols with positivity are compressed sensing protocols," npj quantum inf. **1**, 15018 (2015).
26. A. Peres, *Quantum Theory: Concepts and Methods* (Kluwer, 2002).
27. E. Prugovečki, "Information-theoretical aspects of quantum measurement," Int. J. Theor. Phys. **16**, 321–331 (1977).
28. P. Busch and P. J. Lahti, "The determination of the past and the future of a physical system in quantum mechanics," Found. Phys. **19**, 633–678 (1989).
29. E. J. Candès, "The restricted isometry property and its implications for compressed sensing," C. R. Math. **346**, 589–592 (2008).
30. S. Boyd and L. Vandenberghe, *Convex Optimization* (Cambridge University, 2004).
31. A. Siegman, *Lasers* (Oxford University, 1986).
32. R. W. Gerchberg and W. O. Saxton, "A practical algorithm for the determination of the phase from image and diffraction plane pictures," Optik **35**, 237–246 (1972).
33. A. Ben-Israel and T. N. E. Greville, *Generalized Inverses: Theory and Applications* (Wiley, 1977).
34. A. Luis, "Degree of coherence for vectorial electromagnetic fields as the distance between correlation matrices," J. Opt. Soc. Am. A **24**, 1063–1068 (2007).
35. E. Bolduc, N. Bent, E. Santamato, E. Karimi, and R. W. Boyd, "Exact solution to simultaneous intensity and phase encryption with a single phase-only hologram," Opt. Lett. **38**, 3546–3549 (2013).